

Observable tests of self-interacting dark matter in galaxy clusters: BCG wobbles in a constant density core

David Harvey,^{1,2★} Andrew Robertson³, Richard Massey³ and Ian G. McCarthy⁴

¹Lorentz Institute, Leiden University, Niels Bohrweg 2, NL-2333 CA Leiden, the Netherlands

²Laboratoire d'Astrophysique, EPFL, Observatoire de Sauverny, CH-1290 Versoix, Switzerland

³Institute for Computational Cosmology, Durham University, South Road, Durham DH1 3LE, UK

⁴Astrophysics Research Institute, Liverpool John Moores University, 146 Brownlow Hill, Liverpool L3 5RF, UK

Accepted 2019 June 21. Received 2019 May 23; in original form 2018 December 18

ABSTRACT

Models of cold dark matter (CDM) predict that the distribution of dark matter in galaxy clusters should be cuspy, centrally concentrated. Constant density cores would be strong evidence for beyond CDM physics, such as self-interacting dark matter (SIDM). An observable consequence would be oscillations of the brightest cluster galaxy (BCG) in otherwise relaxed galaxy clusters. Offset BCGs have indeed been observed – but only interpreted via a simplified, analytic model of oscillations. We compare these observations to the BARYONS and HALOES of MASSIVE SYSTEMS (BAHAMAS)–SIDM suite of cosmological simulations, which include SIDM and a fully hydrodynamical treatment of star formation and feedback. We predict that the median offset of BCGs increases with the SIDM cross-section, cluster mass, and the amount of stellar mass within 10 kpc, while CDM exhibits no trend in mass. Interpolating between the simulated cross-sections, we find that the observations (of 10 clusters) are consistent with CDM at the $\sim 1.5\sigma$ level, and prefer cross-section $\sigma/m < 0.12(0.39) \text{ cm}^2 \text{ g}^{-1}$ at 68 per cent (95 per cent) confidence level. This is on the verge of ruling out velocity-independent dark matter self-interactions as the solution to discrepancies between the predicted and observed behaviour of dwarf galaxies, and will be improved by larger surveys by *Euclid* or Super-pressure Balloon-borne Imaging Telescope (SuperBIT).

Key words: gravitational lensing: strong – gravitational lensing: weak – galaxies: clusters: general – dark matter.

1 INTRODUCTION

The search for dark matter remains fruitless. As the dominant mass component in our Universe, revealing its nature has become one of the greatest questions of modern science. However, despite wide efforts to detect it, for example at the Large Hadron Collider in CERN (Kahlhoefer 2017), or directly at the Large Underground Xenon (LUX) experiment (Akerib et al. 2016) the community remains in the dark.

In an effort to diversify and broaden our search, physicists have begun to consider new avenues, focusing on specific properties of dark matter. In this paper, we address one such property, the self-interaction cross-section. Dark matter is commonly assumed to be collisionless. However, dark matter that exhibits a relatively large self-interaction cross-section ($\sigma_{\text{DM}}/m \gtrsim 0.5 \text{ cm}^2 \text{ g}^{-1}$ or $0.2 \text{ barn GeV}^{-1}$) could potentially alleviate problems that exist in the small-scale structure of the standard cold dark matter (CDM) model. By reducing the central densities of dark matter haloes and thus creating a core, it can ease the so-called core-cusp problem

(where observations of dwarf galaxies suggest the existence of cored density profiles where simulations of CDM predict cuspy ones; Dubinski & Carlberg 1991; Yoshida et al. 2000; Davé et al. 2001; Colín et al. 2002; Rocha et al. 2013). It remains unclear whether these inconsistencies are due to unknown baryonic processes or a breakdown in the CDM model. However, it is clear that by constraining self-interacting dark matter (SIDM) we can rule it out as a cause of the small-scale problems, or probe self-interactions in the dark sector, something that is impossible with traditional dark matter experiments.

Efforts to constrain the momentum transfer cross-section per unit mass, σ_{DM}/m have been concentrated mainly on clusters of galaxies. Although some studies have looked at using dwarf galaxies (Zavala, Vogelsberger & Walker 2013; Elbert et al. 2015; Robles et al. 2017), it remains to be seen if these observables are completely discriminative (Strigari, Frenk & White 2017; Harvey et al. 2018). Galaxy clusters, on the other hand, are favourable laboratories in which to probe dark matter self-interactions. The existence of large quantities of dark matter results in strongly deformed space–time meaning that both strong and weak gravitational lensing can be used to infer its distribution.

* E-mail: harvey@lorentz.leidenuniv.nl

Methods that use clusters of galaxies to constrain σ_{DM}/m can be classified into two distinct cases, those using merging clusters and those using relaxed ones. Although initially used due to their apparent simplicity, studies using relaxed clusters suffered from the lack of high-resolution simulations, and hence found it difficult to place reliable constraints (e.g. Miralda-Escudé 2002). As a result, in the past decade attention shifted to merging clusters. By comparing the distribution of dark matter to the collisionless galaxies many studies attempted to constrain the self-interaction cross-section to $\sigma_{\text{DM}}/m \lesssim 1 \text{ cm}^2 \text{ g}^{-1}$ (Markevitch et al. 2004; Randall et al. 2008; Harvey et al. 2015). However, subsequent studies have shown that uncertainties associated with the modelling and measurement interpretation can bias constraints (Robertson, Massey & Eke 2017; Wittman, Golovich & Dawson 2018). It seems that the complex nature of these clusters means that gaining insightful conclusions will require high-resolution simulations and careful modelling.

The key observable that this paper will concentrate on was first proposed by Kim, Peter & Wittman (2017, hereafter K17). They found that during the collision of two equal-mass clusters with cored density profiles, the brightest cluster galaxy (BCG) would become offset from the centre of the halo. A constant central density leads to a gravitational potential that is quadratic in radius. An offset BCG therefore experiences a harmonic oscillation long after the halo has re-relaxed and virialized. It was hypothesized that this observation would not be observed in CDM since the cuspy central region would keep the BCG tightly bound to the centre.

Following this study, an observational paper looking at 10 relaxed galaxy clusters attempted to observe this wobble (Harvey et al. 2017, hereafter H17). They used the parametric gravitational lensing algorithm LENSTOOL to measure the positions of cluster-scale dark matter haloes from the locations of multiply imaged background galaxies, and then measured the separations between the dark matter haloes and their corresponding BCGs. H17 found a wobble of $A_w = 11.8_{-3.0}^{+7.2}$ kpc, where A_w is the amplitude of a harmonic oscillator that parametrizes the distribution of dark matter–BCG offsets. Indeed when compared to n -body simulations, which included realistic baryonic feedback, there appeared to be a 3σ discrepancy with simulations predicting little or no wobble.

Because of a lack of SIDM simulations, H17 were unable to test for systematics associated with the harmonic oscillator model they used to model BCG wobbling. Moreover, the predictions of offset BCGs in K17 were from idealized, dark matter only simulations of equal mass mergers, not cosmological simulations of relaxed clusters. In this paper, we build on these two studies by using cosmological simulations including baryonic physics of both CDM and SIDM, allowing us to characterize the BCG wobbling signal expected with CDM or with different SIDM models.

This paper is structured as follows. In Section 2, we outline the data used, including a recap of the H17 sample, the suite of simulations used, and how we select samples of simulated clusters. The next section outlines how we analyse these samples and we construct our model of the signal. In Section 4, we fit our model, presenting our results, and in Section 5, we discuss our results and give our conclusions.

2 DATA

2.1 Observations

In this paper, we will use the observations from H17 in an attempt to measure the self-interaction cross-section of dark matter. H17 looked at 10 massive galaxy clusters ($\bar{z} = 0.33$), with at least

10 multiple images sourced from the Local Cluster Substructure Survey (LoCuSS; Richard et al. 2010) and the Cluster Lensing And Supernova survey with *Hubble* (CLASH; Zitrin et al. 2015). Using fitted parametric models of the main cluster halo and BCG, they used strong gravitational lensing to estimate the offset between the two in the plane of the sky.

In order to quantify the measurement uncertainty in the positioning due to a finite number of strong lensing constraints, they took the observed multiple images, derived source positions, then using a known model, projected these sources back in to the image plane. Using this new set of multiple images they measured the variance in the estimate of the best-fitting model, finding an rms error of $\sigma_{\text{obs}} = 3.1$ kpc. In this paper, we will adopt the offsets observed along with its associated error estimate.

2.2 Simulations

Our simulations are those introduced in Robertson et al. (2018b), which combined the galaxy formation code BARYONS and HALOES of MASSIVE SYSTEMS (BAHAMAS; McCarthy et al. 2017) with the SIDM code used in Robertson et al. (2017). They were run using a *Wilkinson Microwave Anisotropy Probe* (WMAP) 9-yr cosmology¹ (Bennett et al. 2013).

This paper uses simulations run with four different models of dark matter: CDM (i.e. zero self-interaction cross-section) plus SIDM0.1, SIDM0.3, and SIDM1 (which have velocity-independent cross-sections of 0.1, 0.3, and $1 \text{ cm}^2 \text{ g}^{-1}$, respectively). For each model, we have a $400 h^{-1}$ Mpc box simulated with dark matter and baryon particle masses of 5.5×10^9 and $1.1 \times 10^9 M_{\odot}$, respectively. For CDM and SIDM1 we also have high-resolution simulations of a smaller volume, which we call CDM-hires and SIDM1-hires. The Plummer-equivalent gravitational softening length is $4 h^{-1}$ kpc in physical coordinates below $z = 3$ and is fixed in comoving coordinates at higher redshifts. These have a box size of $100 h^{-1}$ Mpc and eight times better mass resolution than our standard resolution simulations.

The subgrid physics to model the baryonic prescription within the simulations was developed as part of the OWLS project (Schaye et al. 2010). Specifically BAHAMAS includes radiative cooling (Wiersma, Schaye & Smith 2009a), star formation (Schaye & Dalla Vecchia 2008), stellar evolution and chemodynamics (Wiersma et al. 2009b), and stellar and active galactic nucleus (AGN) feedback (Dalla Vecchia & Schaye 2008; Booth & Schaye 2009).

2.3 Matching simulations to observations

In order to sample match those clusters in the suite of simulations and those used in H17 we must separate the relaxed clusters from dynamically unrelaxed. To do so we first take a random sample of 150 friends-of-friends (FoF) clusters with masses $10^{14} < M_{200} < 3 \times 10^{14} M_{\odot}$ and all clusters with $M_{200} > 3 \times 10^{14} M_{\odot}$ over five different redshifts, $z = 0, 0.125, 0.250, 0.375,$ and 0.5 . We choose this separation since there are very few large clusters, but many smaller ones that would computationally take too long to analyse. We then follow the same prescription as in H17 and take the ratio of the X-ray gas emission within 100 and 400 kpc. This gives a proxy for how compact the X-ray gas is, and in the case of relaxed halo with a cool core, this will be high. Studies show that this is good

¹With $\Omega_m = 0.2793$, $\Omega_b = 0.0463$, $\Omega_{\Lambda} = 0.7207$, $\sigma_8 = 0.812$, $n_s = 0.972$, and $h = 0.700$.

Table 1. The sample selection of galaxy clusters from the simulations with their corresponding dark matter cross-section. The third column gives the total number of clusters extracted from the simulation, and the fourth column gives the number of relaxed clusters after cuts. The final column gives the mean halo mass of the cut sample.

Sample	σ_{DM}/m ($\text{cm}^2 \text{g}^{-1}$)	N_{cl}	N_{eff}	$\langle \log(M_{\text{tot}}/M_{\odot}) \rangle$
CDM	0.0	1365	460	14.45
SIDM0.1	0.1	1344	731	14.32
SIDM0.3	0.3	1374	672	14.42
SIDM1	1.0	1330	645	14.40
Obs	N/A	10	10	15.08

proxy for the dynamical state of a cluster with a cut at 0.2 as the divide between relaxed and disturbed (Rasia, Meneghetti & Ettori 2013). Table 1 gives the pre-cut and effective cluster members after we have made our selection.

Having dynamically matched the two samples, we now extract the two components from the simulations: the dark matter and the stellar matter. To do this we run SEXTRACTOR on the projected density distributions. We note here that although this is not directly comparable to observations that use strong gravitational lensing, it does include many sources of error that are of importance. These include the projection effect of cluster members shifting the position, the physics associated with baryons and its coupling to dark matter, the inclusion of outliers that may be included in the sample, for example clusters that appear to be relaxed when in fact they have experienced recent mergers, and any bias due to cluster triaxiality and small haloes close to the centre shifting the halo. Further aspects that are not captured by SEXTRACTOR will be addressed in Section 3.2.

3 METHOD

K17 showed that the BCG of an SIDM galaxy cluster will oscillate in the gravitational potential of a cored density profile. The size of this oscillation should correlate with the core size and hence scale with cross-section. However, this signal is degenerate with the inherent measurement error associated with measuring the centre of a dark matter halo. H17 proposed a solution by modelling the distribution of dark matter–BCG offsets as the convolution of the distribution expected from a harmonic oscillator (with amplitude A_w) with Gaussian measurement errors. To break the degeneracy between these two signals, H17 estimated the measurement errors from fitting Navarro–Frenk–White (NFW) profiles to mock lensing data, generated using known NFW profile lenses. Using this they constrained A_w .

Instead of attempting to break the degeneracy between measurement errors and genuine offsets, we note that the effect of SIDM is simply to broaden the distribution of dark matter–BCG offsets, whether it is wobbling or measurement error. We therefore choose to ignore the physical reason and merely measure the distributions from our simulations, add an additional noise component associated with strong lensing that H17 calculated empirically and then compare the final distributions with the observations.

In order to do this we first infer the positions of the dark matter and the baryonic components using the peak finding algorithm SEXTRACTOR on the projected surface density map of each component. We then model the distribution of offsets between the dark matter halo and the BCG, x with a lognormal probability density function,

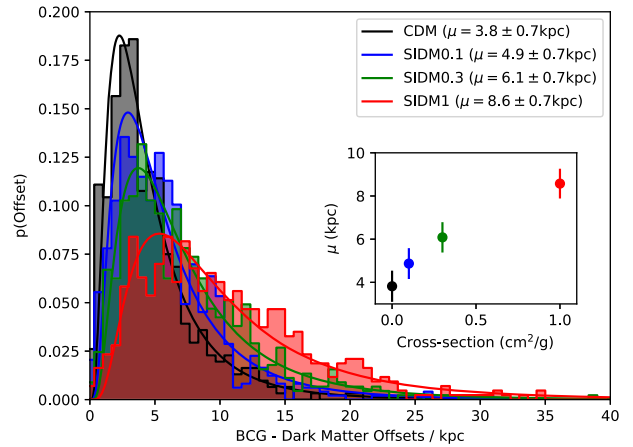


Figure 1. The complete sample of offsets between the brightest cluster galaxy and the dark matter halo for different cross-sections of dark matter. We fit lognormal distributions to each sample and report the median in the legend and the inset axis.

i.e.

$$f(x) = \frac{1}{x\sigma\sqrt{2\pi}} \exp\left(-\frac{(\ln x - \ln \mu)^2}{2\sigma^2}\right), \quad (1)$$

where μ is the median offset and σ^2 its logarithmic variance. We find the best-fitting μ and σ using the maximum likelihood estimator function from SciPy^{2,3}.

It has been noted in previous studies that using a particular algorithm to find the location of projected dark matter haloes can have an impact on the final result (Robertson et al. 2017). This was because in dynamically unrelaxed clusters can produce complex projected dark matter distributions, where different isodensity contours are centred on different points. As such, the position of the dark matter halo changes as a function of the scale on which the position is measured. Here we are dealing with relaxed clusters and therefore should not experience the same effect, however, to test the sensitivity of our results to the choice of algorithm, we study how changing the size of the SEXTRACTOR kernel changes the distribution of offsets. For each simulated cross-section we take a sample of 150 clusters from the $z = 0.25$ snapshot, with masses $M_{200} > 3 \times 10^{14} M_{\odot}$. We then measure μ for a variety of different kernel sizes. We find that the best-fitting μ is insensitive to the choice of kernel size and therefore we are confident that we are measuring an underlying trend and not an artefact of our estimator. Moreover the underlying trend should be independent of the choice of algorithm to find the halo centres. We choose to use a Gaussian kernel with a standard deviation of 9 kpc for the rest of the paper.

We now combine all of the offsets between the BCG and dark matter for each cross-section and measure their lognormal median and variance. Fig. 1 gives the resulting histograms with their best-fitting lognormal distributions and the median of this in the legend and the inset axis.

We find that CDM has the smallest median of $\mu = 3.8 \pm 0.7$ kpc, SIDM0.1, $\mu = 4.9 \pm 0.7$ kpc, SIDM0.3, $\mu = 6.1 \pm 0.7$ kpc, and SIDM1, $\mu = 8.6 \pm 0.7$ kpc.

²<https://docs.scipy.org/doc/scipy/reference/generated/scipy.stats.lognorm.html>

³https://docs.scipy.org/doc/scipy/reference/generated/scipy.stats.rv_continuous.fit.html#scipy.stats.rv_continuous.fit

We find a strong correlation between μ and cross-section. However, if we are to infer the cross-section of dark matter from the observations, we must parametrize how the median offset depends on the cross-section. To do this we follow a forward modelling approach, whereby we take the simulations and apply known effects in order to produce a distribution that can be directly compared to simulations. We therefore state that the total, expected median offset that would be observed, μ_{TOT} is some function of cross-section, σ/m plus some other unknown parameters, i.e.

$$\mu_{\text{TOT}} = g(\sigma/m, X), \quad (2)$$

where X is a list of unknown parameters, which must be identified and then marginalized over. Here we identify three major concerns that will affect how we parametrize this function.

(i) *Finite resolution effects.* The results in Fig. 1 are very close to the gravitational softening length of the simulations, where the gravitational forces become non-Newtonian. In bid to maximize the number of clusters available to the analysis, whilst minimizing computational time, the chosen resolution was selected. However, on scales $r < 10$ kpc, effects could manifest themselves that impact the results. We therefore model any effects that the Plummer softening length of the simulation, ϵ , may have, i.e.

$$\mu_{\text{TOT}} = g(\sigma/m, \epsilon). \quad (3)$$

(ii) *Simulation analysis does not match that of the observations exactly.* The offset between the BCG and dark matter is a combination of the physical wobble and the inherent error in measuring the location of a dark matter halo with a constant density core. In order to compare the simulations directly to the observations, we must either forward model the simulations or deconvolve the expected error distribution from the observations. Given that we are attempting to forward model the simulations through g , we must incorporate the expected effect of observations on the median offset, μ ,

$$\mu_{\text{TOT}} = g(\sigma/m, \epsilon, \hat{\sigma}), \quad (4)$$

where $\hat{\sigma}$ is an operator that will apply observational effects to the offset.

(iii) *Baryonic effects.* It has been recently shown that although more massive dark matter haloes have larger cores (and hence expected to have larger median offsets), those that harbour a larger stellar mass will have a cusper density profile (Kamada et al. 2017; Robertson et al. 2018a). As such, the concentration of stellar mass and the halo mass will likely impact the median offset given the scales in question and hence we must incorporate in to our final ansatz,

$$\mu_{\text{TOT}} = g(\sigma/m, \epsilon, \hat{\sigma}, M_{200}, M_{\star}). \quad (5)$$

The following sections will investigate each of these components further.

3.1 Accounting for finite simulation resolution

Our initial analysis of the simulations shows that the expected median dark matter–BCG offset is $\mu \sim 10$ kpc and is therefore in proximity to the Plummer-equivalent gravitational softening length of the simulations ($\epsilon = 4 h^{-1}$ kpc; Springel 2005). We therefore investigate how sensitive these results are to the resolution of the simulations. H17 found a significant difference between the low- and high-resolution simulations for CDM, and hence the ~ 4 kpc offset observed in CDM could be just the sensitivity limit of the

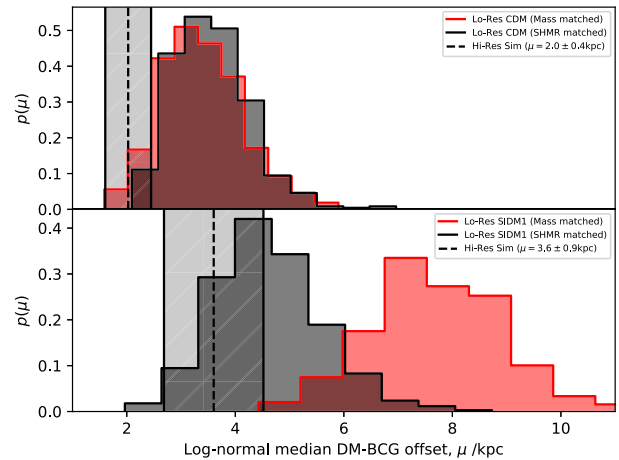


Figure 2. Effect of finite resolution. We test whether high- and low-resolution simulations of the same simulation produce similar results given a similar mass distribution (red histogram) and sample size or similar stellar to halo mass ratio (black histogram). Given that the low-resolution sample has many more haloes than the high resolution we randomly sample the same number of clusters as in the high resolution and measure μ . The dotted vertical line shows the estimate from the hires simulation with the associated error bar given by the shaded region. We find the estimated median in the high resolution is underpredicted compared to that of the low resolution and therefore must be modelled.

simulation, which could also be impacting the other simulations. We therefore run two smaller, high-resolution boxes, one for CDM and one for SIDM1, and compare the predicted signals.

To do this, we first measure the best-fitting μ for the CDM and SIDM1-hires sample of ~ 20 clusters, selected using the procedure described in Section 2.3. We then generate a mass-matched sample also of ~ 20 clusters from the CDM and SIDM1 simulation, and measure μ for these samples. Given the large volume of the low-resolution simulations, we can generate many such samples, and so we repeat this second step 300 times. Fig. 2 shows the results. The red filled histograms show the measured distribution of μ from the 300 CDM (top panel) and SIDM1 (bottom panel) samples. The dotted vertical line and shaded region give the measured value and error from the high-resolution sample. We find that the high-resolution simulations in both situations have lower medians compared to the low resolution.

Looking closely at the density profiles of each sample, we find that the high-resolution haloes have denser stellar profiles than their low-resolution counterparts. In galaxy clusters with SIDM, denser stellar distributions lead to smaller dark matter cores (Robertson et al. 2018a), so in order to understand the differences due to *only* the resolution (and not due to differences arising from different baryon distributions), we match the samples in stellar to halo mass ratio (SHMR) and recalculate the distribution. The result is the black solid histograms in Fig. 2. We find that by matching the samples in SHMR, the agreement between the low- and high resolution is improved, however there remains some residual difference. We therefore apply very strict SHMR matching such that there are equal number of clusters in each low- and high-resolution sample and model the effect of the softening via the ansatz,

$$\mu_{\text{MEAS}} = (\mu_{\text{SIM}}^{\gamma} + (\alpha\epsilon)^{\gamma})^{\frac{1}{\gamma}}, \quad (6)$$

where μ_{MEAS} and μ_{SIM} are the measured and intrinsic lognormal medians for a particular cross-section, and ϵ is the softening length

of the simulation. Using two different resolution simulations, from two different cross-sections (i.e. high and low res for SIDM1 and CDM), we are able to fit for the four parameters, γ , α , $\mu_{\text{SIM,CDM}}$, and $\mu_{\text{SIM,SIDM1}}$. Once we have found γ and α , we are able to calculate μ_{SIM} for any low- or high-resolution simulation (assuming that these values are constant for other cross-sections and halo masses).

3.2 Applying observational effects

In order to fully forward model the simulations in order to directly compare with observations, we must add an additional source of error. However carrying out a full mock gravitational lensing analysis on the simulated clusters is beyond the scope of this paper and therefore we choose to numerically modify μ_{SIM} .

Instead we convolve the effect of observational noise on to the simulation data by numerically adding random Gaussian noise to each radial offset in the measured lognormal distributions. We then remeasure the lognormal distributions. Since we do this numerically, to get accurate results it takes some time. Therefore in order to speed this up we test whether this numerical method has an analytical form. Given that in all sense this is just a convolution of a lognormal radial and delta function with a Gaussian distribution, it is not possible to calculate analytically. We therefore carry out some mock tests with a known lognormal, add on the observational noise, and recalculate the median. As Fig. 3 shows, we find that the resulting median is almost exactly the sum of the original median and the width of the Gaussian, added in quadrature.

We therefore choose to model the effect of observational noise on the median offsets by adding them in quadrature, i.e.

$$\mu_{\text{TOT}}^2 = \mu_{\text{SIM}}^2 + \sigma_{\text{obs}}^2. \quad (7)$$

3.3 The impact of baryons on the dark matter

Initial studies clearly showed the expected offsets were well within the stellar distribution of the BCG. Thus subgrid physics models that may affect the distribution of stellar matter will likely impact the signal we observe. This hypothesis was backed up when we noticed the difference in expect median offset between a mass-matched sample and a sample matched in SHMR in the previous section.

How the baryons impact our results will primarily depend on how well the BAHAMAS simulation do at reproducing the observed stellar mass distribution. The BAHAMAS simulations have been tuned to return the correct stellar mass function, and as such the observed H17 cluster sample SHMR relation *should* match the simulated one. If this is the case, then constraints derived from a representative sample should be unbiased. Using stellar masses from Burke, Hilton & Collins (2015), we find that indeed this is the case, and the SHMR of the observed clusters well matches the simulated ones.

However, the stellar mass is measured up to ~ 50 kpc, well beyond the scales that are probed by this technique, which are closer to ~ 10 kpc. This is particularly important since although the simulations have been tuned to give the correct total stellar mass, the amount of stellar mass on the scales in question could be very different. As such we look closer at the distribution of stellar mass within ~ 10 kpc. Using estimates from DeMaio et al. (2018), we find that in fact the observed clusters have a much high density of stellar mass within 10 kpc. As such we are motivated to model the behaviour of the median offset as a function of halo mass *and* stellar

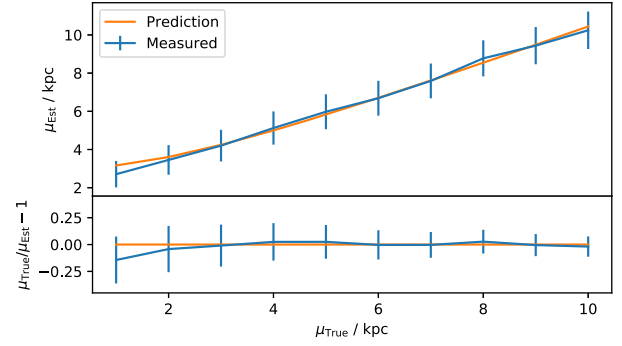


Figure 3. The effect of convolving a lognormal distribution with a Gaussian of width $\sigma_{\text{obs}} = 3.1$ kpc. The prediction is the simply the μ_{SIM} added in quadrature with the observational noise.

mass within 10 kpc:

$$\begin{aligned} \mu_{\text{SIM}} = & X_1 + X_2 \log_{10} \left(\frac{M_{200}}{10^{14} M_{\odot}} \right) \\ & + X_3 \log_{10} \left(\frac{M_{*}(< 10 \text{ kpc})}{10^{11} M_{\odot}} \right), \end{aligned} \quad (8)$$

where the relation to cross-section could be either

$$X_i(\sigma) = a_i + b_i \log_{10} \left(\frac{\sigma/m}{1 \text{ cm}^2 \text{ g}^{-1}} \right) \text{ for } i = 1, 2 \quad (9)$$

or

$$X_i(\sigma) = a_i + b_i \left(\frac{\sigma/m}{1 \text{ cm}^2 \text{ g}^{-1}} \right) \text{ for } i = 1, 2. \quad (10)$$

Following this we carry out the second fit using a least squares and a modified loss function to determine a_i and b_i ;

$$\chi^2 = \sum_{i=0}^{n_{\text{Sim}}} \frac{(\tilde{\mu}_{\text{SIM}_i} - \mu_{\text{SIM}_i})^2}{\sigma_{\text{SIM}_i}}, \quad (11)$$

where $\tilde{\mu}_{\text{SIM}_i}$ is the model median value and μ_{SIM_i} is the actual measured median value for the i th cross-section. In the case where we assume a log cross-section ansatz, we sum over only finite cross-sections, whereas for a model linear in cross-section we include also CDM.

In order to choose between a linear or log cross-section model, we compute the Bayesian information criterion (BIC), which penalizes any good fit by the number of parameters used in the model in an attempt to reduce overfitting. The BIC can be computed by

$$\text{BIC} = -2 \ln(L) + k \ln(n), \quad (12)$$

where L is the likelihood of the maximized model, n is the total number of data points, and k is the number of parameters. We give the corresponding BIC for each model in the fifth column of Table 3. We find $\Delta\text{BIC} = 4$ between the two models, which corresponds to a preference for the log model. We therefore adopt this model and show it in Fig. 4 with individual models in the right-hand panel.

4 RESULTS

Following the construction of our model, we have a total of 10 *non*-independent parameters:

$$\theta = \{\mu_{\text{SIM,CDM}}, \mu_{\text{SIM,SIDM1}}, \alpha, \gamma, a_1, b_1, a_2, b_2, a_3, b_3\}. \quad (13)$$

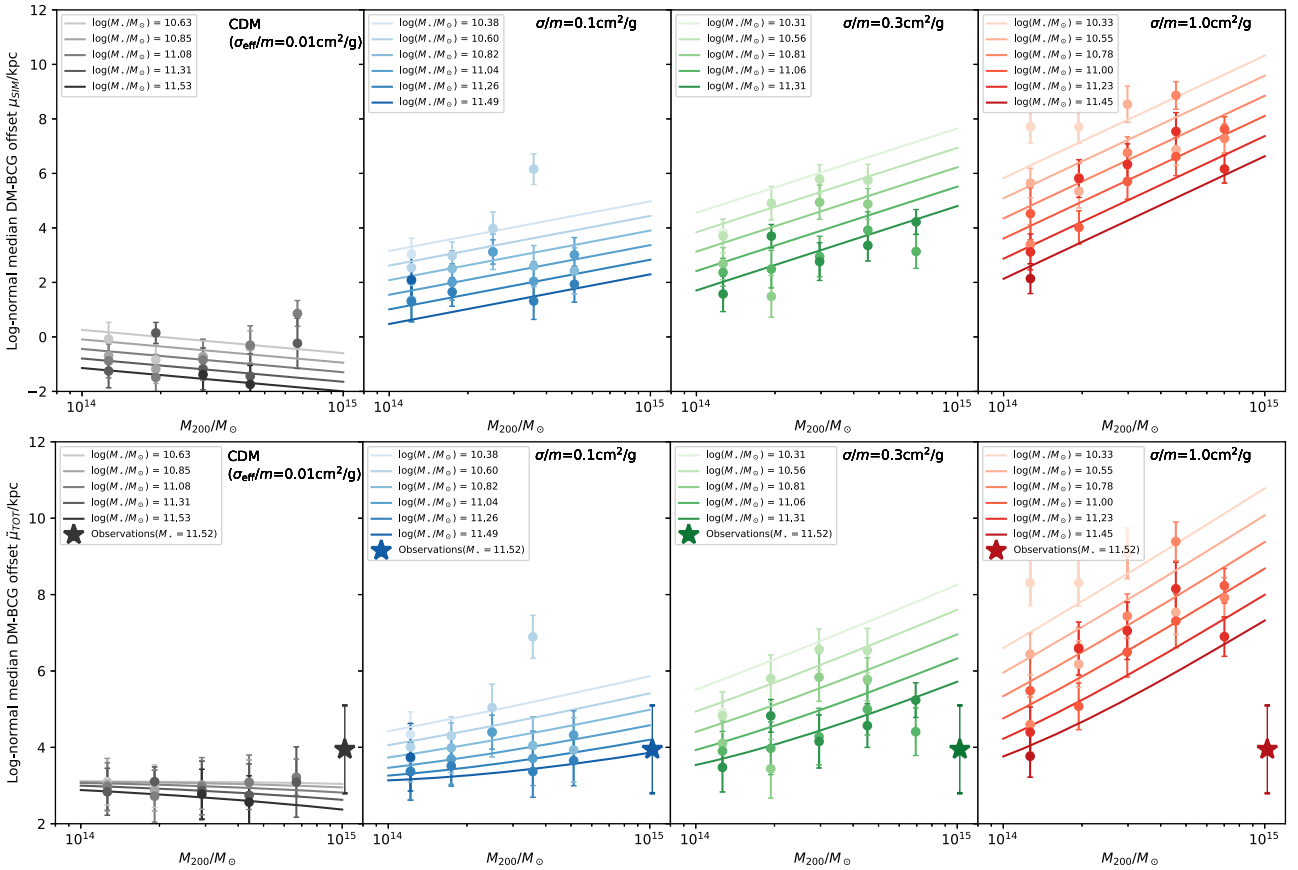


Figure 4. Our final model for the observed offset between the BCG and dark matter in relaxed clusters, as a function of the halo mass, stellar mass within 10 kpc (different lines), and self-interaction cross-section of dark matter, $\sigma_{\text{DM}}/m = 0, 0.1, 0.3, 1.0$ from left to right, in the absence of any experimental noise (top) and with observational noise (bottom). For comparison we show the observations in the bottom row with a star and the colour representing the stellar mass (also shown in the legend). Since we assume a model in $\log \sigma$, where CDM is ill-defined, we show the effective cross-section of our model. This represents the validity limit $\sigma/m = 0.01 \text{ cm}^2 \text{ g}^{-1}$.

Table 2. The fitted parameters to equation (6), where we model the effect of the finite resolution of the simulation on our results. We also find that $\alpha = 0.41^{+0.37}_{-0.01}$ and $\log_{10}(\gamma) = -0.02^{+0.61}_{-0.01}$.

Sample	$\mu_{\text{MEAS, lo}}$ (kpc)	$\mu_{\text{MEAS, hi}}$ (kpc)	μ_{SIM} (kpc)
CDM	3.80 ± 0.7	2.0 ± 0.4	$0.8^{+0.9}_{-0.8}$
SIDM1	5.0 ± 1.0	3.6 ± 0.9	$2.3^{+1.8}_{-0.7}$

They are not independent since the estimate of the softening model parameters will affect the following a_i and b_i . As such we carry out the fit to the four softening model parameters first using a least-squares algorithm. Table 2 gives the results of the fit.

We show the final model in Fig. 5. The top row shows the best-fitting model for the three finite cross-sections. In each panel we show the model estimate $\tilde{\mu}_{\text{SIM}}$ as the solid lines and the actual measured estimate μ_{SIM} as the data points to which the model is fitted, as a function of halo mass and stellar mass within 10 kpc. The bottom row shows the total, expected model, μ_{TOT} after adding observational noise. We estimate the median offset of the H17 sample of clusters finding that $\mu_{\text{obs}} = 3.9 \pm 1.2$ kpc. We show this estimate as the star in each panel, where the colour of the star and legend gives the estimated stellar mass. The corresponding model parameters can be found in Table 3.

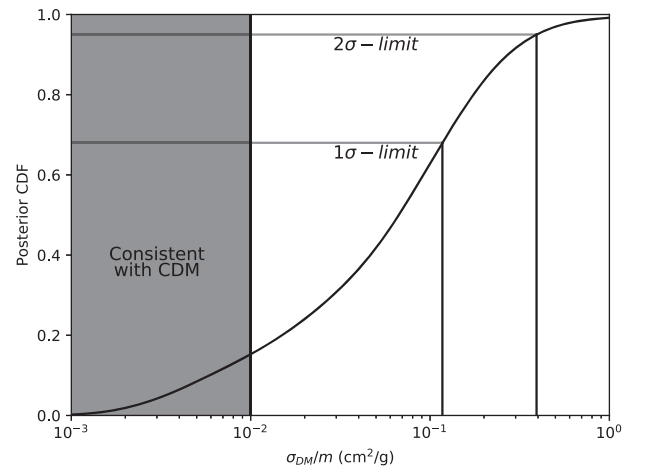


Figure 5. The cumulative probability distribution of the observations given our model (assuming equation 9), folding in errors associated with the parameters in equation (6). We give the 1σ and 2σ limits of the observations that correspond to $\sigma_{\text{DM}}/m < 0.12(0.39) \text{ cm}^2 \text{ g}^{-1}$ at 68 per cent (95 per cent) confidence limit. Given that in this model CDM ($\sigma/m = 0 \text{ cm}^2 \text{ g}^{-1}$) is undefined, we estimate the validity limit of the model, and the sensitivity limit of the simulations. The CDM offsets can be interpreted as $\sigma_{\text{CDM}} = 0.01 \text{ cm}^2 \text{ g}^{-1}$ and is given by the shaded region. We find that 15 per cent of the probability of the observations lie in this region, hence showing that the observations are in tension with CDM at the $\sim 1.5\sigma$ level.

Table 3. The fitted coefficients to equations (9) and (10), where we model the BCG–dark matter offset as a function of mass, stellar mass, and cross-section. The sixth column shows the Bayesian information criterion (BIC) that allows a comparison of the two models. With a $\Delta\text{BIC} = 4$ there is a preference for a log cross-section model.

Model	a_1 (kpc)	b_1 (kpc)	a_2 (kpc)	b_2 (kpc)	a_3 (kpc)	b_3 (kpc)	BIC
Log	4.5 ± 0.4	2.7 ± 0.8	3.6 ± 0.2	2.0 ± 0.4	-3.3 ± 0.4	-0.9 ± 0.7	62
Linear	1.9 ± 0.4	2.6 ± 0.7	1.4 ± 0.2	2.4 ± 0.3	-2.1 ± 0.3	-1.3 ± 0.6	66

Given that CDM ($\sigma_{\text{DM}}/m = 0$) is not defined in this logarithmic model, however, gives a finite offset, we calculate what the effective cross-section the offsets predict in this model. This cross-section represents the sensitivity and validity limit of the simulations. We find that the effective cross-section of CDM is $\sigma_{\text{DM}}/m = 0.01 \pm 0.007 \text{ cm}^2 \text{ g}^{-1}$.

4.1 Constraints on the self-interaction cross-section

We now use the fitted models to directly constrain the cross-section of dark matter. In order to do this we must fold in the uncertainties of our model mainly driven by the softening model, since all subsequent parameters are derived from these. To do this we carry out the following prescription.

(i) We first draw a sample randomly from the estimates of $\mu_{\text{SIM}, \text{lo}}$ and $\mu_{\text{SIM}, \text{hi}}$ (from Table 2), sampling from Gaussian distributions centred on the quoted means and with widths (standard deviations) given by the quoted errors.

(ii) From these estimates, we rederive the four softening model parameters (equation 6).

(iii) Using the newly generated softening model we refit for μ_{SIM} via equations (8) and (11) and add observational noise to get a model of μ_{TOT} .

(iv) Assuming a Gaussian probability density distribution in μ_{obs} , we calculate the cumulative density distribution (CDFs) in σ/m using our new model of μ_{TOT} , adopting stellar mass estimates from DeMaio et al. (2018).

(v) Repeating 10^3 times, we generate multiple CDFs and then take the mean to get the final CDF.

The final mean CDF can be found in Fig. 5 corresponding to an upper limit of $\sigma_{\text{DM}}/m < 0.12$ (0.39) $\text{cm}^2 \text{ g}^{-1}$ 68 per cent (95 per cent). We find that 15 per cent of the probability lies below the sensitivity threshold of the simulations ($\sigma_{\text{DM}}/m < 0.01 \text{ cm}^2 \text{ g}^{-1}$), and is therefore consistent with CDM. This limit is illustrated by the shaded region.

4.2 Future prospects

This study has shown that with only a small number of strong lensing galaxy clusters we are able to place tight constraints on the self-interaction cross-section of dark matter. With future studies soon to come online we investigate how this method scales statistically. To this end we calculate the predicted 95 per cent constraints for two future studies: Super-pressure Balloon-borne Imaging Telescope (SuperBIT), a balloon-borne telescope that will image 200 galaxy clusters (Romualdez et al. 2016), and *Euclid* (Laureijs et al. 2011), a space-based telescope that will image $\sim 10^3$ – 10^5 clusters. We calculate the constraints as a function of the average error in a single cluster, σ_{obs} . To do this we take the H17 value and error and reduce the error by a factor of $\sqrt{N_{\text{cl}}}$, and shift the median, μ , for different values of σ_{obs} . Fig. 6 shows the results. Each dotted line

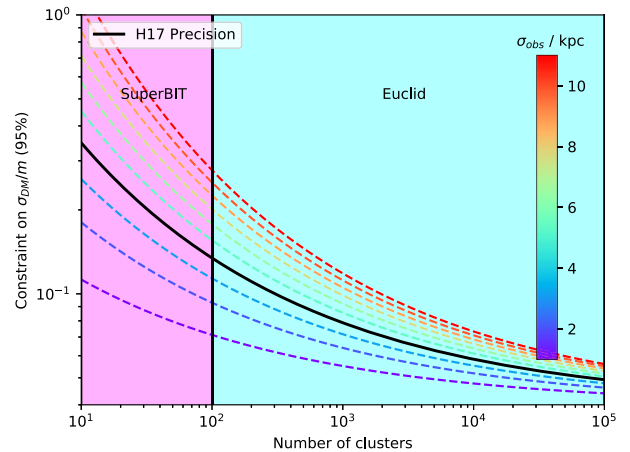


Figure 6. Forecasted 95 per cent confidence limits for future surveys as a function of the number of clusters and the precision of a single cluster estimate. SuperBIT and *Euclid* will observe of order 10^2 and 10^5 clusters, respectively. The solid black line is the precision found in H17, for observations of strong gravitational lensing by 10 clusters. We find that although SuperBIT will yield a factor of ~ 2 improvement, large surveys like *Euclid* will only bring diminishing returns. Interestingly, even weak lensing observations with a precision on dark matter astrometry of only ~ 10 kpc may be able to place discriminating constraints in the future.

is a study with increasing precision on a single cluster. The solid cyan line is the sensitivity of this study, and the sensitivity regions of each survey are given in pink (cyan) for SuperBIT (*Euclid*). We find that although an initial increase in sample size will improve the constraints by a factor of ~ 2 , further improvements would be moderate. As such, this experiment would be ideal for a survey the size of SuperBIT. A precision on dark matter astrometry of ~ 10 kpc, which can be achieved with weak gravitational lensing, will place discriminatory constraints and therefore could be of interest in the future.

5 DISCUSSION AND CONCLUSIONS

We have used cosmological simulations of CDM and SIDM that include realistic baryonic physics to constrain the velocity independent, elastic, self-interaction cross-section of dark matter.

It is predicted that during the collision of two galaxy clusters that harbour cored density profiles, the BCG will be initially offset from the centre of the halo. Long after the relaxation of the cluster, this offset can persist with the BCG tracing out the motion of a harmonic oscillator (K17). In CDM, the central density profile is cuspy and hence the BCG will be bound tight to the centre of the dark matter halo, however, in models of dark matter that predict cores this will be a clear signal for a non-standard model of dark matter.

In a recent paper, the distribution of offsets between the BCG and dark matter halo was estimated in 10 galaxy clusters. Fitting a two-

component model they estimated that the wobble amplitude, $A_w \sim 11$ kpc (H17), in close agreement with previous studies (Newman et al. 2013). They compared this to high-resolution simulations of CDM and found a discrepancy at the $\sim 3\sigma$ level.

In this paper, we have extended this comparison to include simulations with velocity-independent dark matter self-interactions. The simulations were run with four different cross-sections: $\sigma_{DM}/m = 0$ (CDM), 0.1, 0.3, and $1.0 \text{ cm}^2 \text{ g}^{-1}$. Modelling the distribution of BCG–dark matter offsets as a lognormal, we found that the median offset, μ , increased with cross-section: $\mu_{\text{CDM}} = 3.8 \pm 0.7$ kpc, $\mu_{0.1} = 4.9 \pm 0.7$ kpc, $\mu_{0.3} = 6.1 \pm 0.7$ kpc, and $\mu_{1.0} = 8.6 \pm 0.7$ kpc.

In order to infer the cross-section of dark matter from the simulations, we construct a model that relates the median offset to the cross-section. We identify three clear concerns that are folded into this model:

- (i) the effect of the close proximity of the signal to the finite smoothing length of the simulation;
- (ii) the effect of observational noise on the signal;
- (iii) the impact of baryons in the core of the cluster.

Parametrizing each, we estimate the final cross-section of dark matter, finding that $\sigma_{DM}/m < 0.12$ (0.39) $\text{cm}^2 \text{ g}^{-1}$ 68 per cent (95 per cent). Under the assumption that the model scales with the log of the cross-section, CDM is undefined. We therefore use the CDM simulations to estimate the validity limit of this model and the sensitivity limit of the simulations. We find that the offsets observed in CDM are interpreted as an effective cross-section of $\sigma/m = 0.01 \text{ cm}^2 \text{ g}^{-1}$. Given our observations, we find that 15 per cent of the probability lies within this region and hence the observations are consistent with CDM to within $\sim 1.5\sigma$.

The consequence of this limit is that models of SIDM that can significantly alter the structure of dwarf galaxy dark matter haloes would require a cross-section that varies with the relative velocity between dark matter particles. With observations of just 10 galaxy clusters, this method is almost at the precision necessary to discriminate between (and potentially rule out) otherwise viable models of dark matter. Future surveys, such as observations by SuperBIT of weak lensing around ~ 200 clusters, will soon have the power to make dramatic impact.

ACKNOWLEDGEMENTS

This research is supported by the Swiss National Science Foundation (SNSF). DH acknowledges support by the Merac foundation and the ITP Delta foundation. AR is supported by the European Research Council (ERC-StG-716532-PUNCA) and the UK STFC (ST/N001494/1). RM is supported by a Royal Society University Research Fellowship. This project has received funding from the European Research Council (ERC) under the European Union’s Horizon 2020 research and innovation programme (grant agreement no. 769130). We would also like to thank Joop Schaye for his contributions to the BAHAMAS simulations. This work used the DiRAC Data Centric system at Durham University, operated by the Institute for Computational Cosmology on behalf of the STFC DiRAC HPC Facility (www.dirac.ac.uk). This equipment was funded by BIS National E-infrastructure capital grant ST/K00042X/1, STFC capital grants ST/H008519/1 and ST/K00087X/1, STFC DiRAC

Operations grant ST/K003267/1, and Durham University. DiRAC is part of the National E-Infrastructure.

REFERENCES

- Akerib D. S. et al., 2016, *Phys. Rev. Lett.*, 116, 161302
 Bennett C. L. et al., 2013, *ApJS*, 208, 20
 Booth C. M., Schaye J., 2009, *MNRAS*, 398, 53
 Burke C., Hilton M., Collins C., 2015, *MNRAS*, 449, 2353
 Colín P., Avila-Reese V., Valenzuela O., Firmani C., 2002, *ApJ*, 581, 777
 Dalla Vecchia C., Schaye J., 2008, *MNRAS*, 387, 1431
 Davé R., Spergel D. N., Steinhardt P. J., Wandelt B. D., 2001, *ApJ*, 547, 574
 DeMaio T., Gonzalez A. H., Zabludoff A., Zaritsky D., Connor T., Donahue M., Mulchaey J. S., 2018, *MNRAS*, 474, 3009
 Dubinski J., Carlberg R. G., 1991, *ApJ*, 378, 496
 Elbert O. D., Bullock J. S., Garrison-Kimmel S., Rocha M., Oñorbe J., Peter A. H. G., 2015, *MNRAS*, 453, 29
 Harvey D., Massey R., Kitching T., Taylor A., Tittley E., 2015, *Science*, 347, 1462
 Harvey D., Courbin F., Kneib J. P., McCarthy I. G., 2017, *MNRAS*, 472, 1972 (H17)
 Harvey D., Revaz Y., Robertson A., Hausammann L., 2018, *MNRAS*, 481, L89
 Kahlhoefer F., 2017, *Int. J. Modern Phys. A*, 32, 1730006
 Kamada A., Kaplinghat M., Pace A. B., Yu H.-B., 2017, *Phys. Rev. Lett.*, 119, 111102
 Kim S. Y., Peter A. H. G., Wittman D., 2017, *MNRAS*, 469, 1414 (K17)
 Laureijs R. et al., 2011, preprint([arXiv:1110.3193](https://arxiv.org/abs/1110.3193))
 McCarthy I. G., Schaye J., Bird S., Le Brun A. M. C., 2017, *MNRAS*, 465, 2936
 Markevitch M., Gonzalez A. H., Clowe D., Vikhlinin A., Forman W., Jones C., Murray S., Tucker W., 2004, *ApJ*, 606, 819
 Miralda-Escudé J., 2002, *ApJ*, 564, 60
 Newman A. B., Treu T., Ellis R. S., Sand D. J., Nipoti C., Richard J., Jullo E., 2013, *ApJ*, 765, 24
 Randall S. W., Markevitch M., Clowe D., Gonzalez A. H., Bradač M., 2008, *ApJ*, 679, 1173
 Rasia E., Meneghetti M., Ettori S., 2013, *Astron. Rev.*, 8, 40
 Richard J. et al., 2010, *MNRAS*, 404, 325
 Robertson A., Massey R., Eke V., 2017, *MNRAS*, 465, 569
 Robertson A. et al., 2018a, *MNRAS*, 476, L20
 Robertson A., Harvey D., Massey R., Eke V., McCarthy I. G., Jauzac M., Li B., Schaye J., 2018b, preprint([arXiv:1810.05649](https://arxiv.org/abs/1810.05649))
 Robles V. H. et al., 2017, *MNRAS*, 472, 2945
 Rocha M., Peter A. H. G., Bullock J. S., Kaplinghat M., Garrison-Kimmel S., Oñorbe J., Moustakas L. A., 2013, *MNRAS*, 430, 81
 Romualdez L. J. et al., 2016, preprint([arXiv:1608.02502](https://arxiv.org/abs/1608.02502))
 Schaye J., Dalla Vecchia C., 2008, *MNRAS*, 383, 1210
 Schaye J. et al., 2010, *MNRAS*, 402, 1536
 Springel V., 2005, *MNRAS*, 364, 1105
 Strigari L. E., Frenk C. S., White S. D. M., 2017, *ApJ*, 838, 123
 Wiersma R. P. C., Schaye J., Smith B. D., 2009a, *MNRAS*, 393, 99
 Wiersma R. P. C., Schaye J., Theuns T., Dalla Vecchia C., Tornatore L., 2009b, *MNRAS*, 399, 574
 Wittman D., Golovich N., Dawson W. A., 2018, *ApJ*, 869, 104
 Yoshida N., Springel V., White S. D. M., Tormen G., 2000, *ApJ*, 544, L87
 Zavala J., Vogelsberger M., Walker M. G., 2013, *MNRAS*, 431, L20
 Zitrin A. et al., 2015, *ApJ*, 801, 44

This paper has been typeset from a $\text{\TeX}/\text{\LaTeX}$ file prepared by the author.